Science Press

ARTICLE

Influence of Temperatures on Creep Behavior of Pt-Al Coated Third-Generation Low-Cost Single Crystal Superalloy

Zhang Ge[1],   Tao Xipeng[2],   Syed Muhammad Abbas Jafri[2],   Wang Xinguang[2],   Zhang Song[1],
Zhang Chunhua[1],   Liang Jingjing[2],   Li Jinguo[2],   Sun Xiaofeng[2],   Zhou Yizhou[2]

[1] School of Materials Science and Engineering, Shenyang University of Technology, Shenyang 110870, China; [2] Shi-Changxu Innovation Center for Advanced Materials, Institute of Metal Research, Chinese Academy of Sciences, Shenyang 110016, China

Abstract: The influence of applied temperatures on the creep rupture life of the third-generation low-cost single crystal (SX) superalloy with Pt-Al coating was evaluated. The creep damage was observed under the conditions of 1100 °C/137 MPa, 1120 °C/137 MPa, and 1140 °C/137 MPa. Results show that the properties of bare superalloy outperform those of coated superalloy under all test conditions. The most significant reduction in creep life reaches 50% when the test condition is 1100 °C/137 MPa. At higher temperatures (1120 and 1140 °C), the crack propagation rate in Pt-Al coatings to SX superalloy substrate decreases, thereby reducing the degradation degree of mechanical properties. Instead of the penetration into SX substrate, tip oxidation and Al diffusion of the coating cracks cause the formation of oxides, therefore leading to the slow degradation in microstructures of the substrate beneath the coating. At 1100 °C, however, the microstructure of coating/SX superalloy substrate degrades due to the Al internal diffusion. This diffusion mechanism promotes the formation of harmful topologically close packed phases around 1100 °C. At 1120 and 1140 °C, the dislocation of SX superalloy substrate beneath the coating is relatively unchanged, compared to that in the inner superalloy. In contrast, the dislocation network of the substrate beneath the coating becomes sparse, and the number of superdislocations cutting into γ' phases increases at 1100 °C.

Key words: Pt-Al coating; high-temperature creep; single crystal superalloy; crack oxidation; microstructure evolution

High-temperature components in the aircraft engine frequently encounter oxidization and hot corrosion resistance due to the thermal exposure. Protective coatings are applied to prevent high-temperature damage. During high-temperature operation, platinum-modified aluminide (Pt-Al) coatings can improve oxidation resistance and hot corrosion resistance in nickel-based superalloy components, such as blades and veins[1–4]. At elevated temperatures, the Pt-Al coating are transformed into dense and adherent alumina layer. This process contributes to the exceptional oxidation resistance of coatings[5–7]. In gas turbine installations, the process of cyclic heating and cooling is common, which leads to scale spallation. However, Pt coatings improve the scale adhesion and reduce the incidence of scale spallation[8–10]. Consequently, these coatings exhibit significantly increased effectiveness against the exposure at high temperatures and under oxidation conditions.

Despite the fact that Pt-Al coatings provide excellent oxidation resistance to single crystal (SX) substrates, they deteriorate the mechanical properties of the superalloy substrates[11–13]. The external layer of the coating is primarily composed of the brittle β-NiAl phase because of degradation. Generally, the ductile-to-brittle transition temperature (DBTT) is above 650 °C[14]. Aluminide coatings can impact various mechanical properties of superalloys, such as tensile strength[15], creep resistance[16], high cycle fatigue performance[17], and thermo-mechanical fatigue resistance[18]. Li et al[19] reported that the strength of CMSX-2 SX alloy was unaffected even at 1050 °C after applying aluminide coatings. However, the coating causes a significant reduction in the ductility of alloys

at room temperature. However, the coated alloys show exceptionally high ductility at 850 °C[20]. Lei et al[21] investigated the effect of Pt-Al coating on the tensile properties of directionally solidified CM-247LC superalloy at 870 °C. The characteristics of the coated and uncoated superalloys were analyzed after cyclic oxidation process at 1100 °C in air. The coating had a negative impact on the strength of the base alloy, which was reduced by 8%–10%, but its ductility was not significantly affected. After cyclic oxidation exposure at 1100 °C for 750 h, the ductility of the coated superalloys was considerably higher than that of the uncoated superalloy[22].

The effect of aluminide coatings on the creep and stress fracture behavior of superalloys is rarely reported. It is commonly reported that the presence of aluminizing diffusion coating does not affect the fracture life of the substrate. Besides, the tests are often conducted above DBTT of the coating[23]. Zhang et al[24] found that applying Pt-Al bonding layer on CM-247LC Ni-based superalloy could reduce the creep rupture life by over 45%. It is reported that the presence of Pt-Al bonding layer shortens the thermo-mechanical fatigue life of superalloys. Although several studies were performed on the mechanical characteristics of superalloys with aluminizing diffusion coating, comprehensive investigation about the impact of Pt-Al coating on the creep behavior of superalloy substrates at different high temperatures is rarely conducted.

One criterion to evaluate the high-temperature performance of superalloys is the highest temperature, at which the superalloy can bear creep test at 137 MPa for 1000 h[25]. In order to shorten the experiment period and reduce cost, accelerated experiments were conducted by increasing the temperature. In previous research, the second-generation nickel-based SX superalloy DD5 containing 3% Re was tested under the 1100 °C/137 MPa condition, and the results are considered as the benchmark. Then, the change in properties was measured at even higher temperatures (1120 and 1140 °C)[26]. The service temperature of the third-generation nickel-based SX superalloy is 1120 °C. Considering the acceleration and deceleration flight motions of the aero-engine, the mechanical properties of SX superalloy at 1140 °C should also be investigated.

In this research, the impact of Pt-Al coatings on the creep behavior of third-generation SX superalloys at high temperatures ranging from 1100 °C to 1140 °C was studied. This study involved the in-depth microstructure and morphology analyses of test samples under both uncoated and coated conditions to gain a comprehensive understanding of high-temperature creep behavior of superalloys. This research

provided valuable insights into the potential applications of Pt–Al bonding coatings for the performance enhancement of superalloys in high-temperature environments.

1 Experiment

The low-cost third-generation SX superalloy was employed as the substrate, which was cast into ingots with 15 mm in diameter. The crystallographic orientation was along [001] direction. The standard chemical composition of SX superalloy substrate is shown in Table 1.

To facilitate the formation of the ordered γ-γ' structure in the substrate, solid solution treatment was performed to homogenize the substrate, followed by a two-stage aging treatment under vacuum condition. The comprehensive standard heat treatment procedure is presented in Table 2. Samples with diameter of 5 mm and gauge length of 27 mm were machined for creep tests, as shown in Fig. 1. After grinding with 240#–3000# SiC sandpaper, the substrates were ultrasonically cleaned in alcohol.

The coating process involved two steps. The first step was depositing Pt through electroplating. A pure Pt plate anode was used during the coating process and the pH value was 7–11. Electroplating was conducted at current density from 1 A/dm² to 5 A/dm² and the temperature was between 60 and 90 °C. Afterwards, a Pt layer with thickness of 6 μm was obtained. Subsequently, the plated Pt sample underwent vacuum annealing in furnace at 1040 °C for 1 h with vacuum level higher than 6×10^{-3} Pa and heating rate of 5 °C/min. The second step involved the deposition of Al layer onto the annealed Pt-coated sample using vapor deposition method. The aluminizing diffusion treatment was conducted under vacuum condition at 1070 °C for 5 h. The Pt-Al coating preparation process was outlined in Ref.[27].

Creep tests were performed in air at 1100, 1120, and 1140 °C under the applied stress of 137 MPa until complete fracture. The testing conditions of 1100 °C/137 MPa, 1120 °C/137 MPa, and 1140 °C/137 MPa were designated as T1, T2, and T3 conditions, respectively. The SWGH7.16-J11B apparatus was used to conduct the creep rupture tests. Along the gauge length, the temperature variation of ±1.0 K was maintained. Additionally, the samples were examined by strain-displacement sensor equipment in conjunction with high-temperature extensometer.

Table 1 Nominal chemical composition of SX superalloy substrate (wt%)

Cr	Co+Mo+W	Re	Al	Ta	Ni
4.6	18.0	3.0	5.9	6.0	Bal.

Table 2 Standard heat treatment procedure of SX superalloy in this research

Specific step	Standard heat treatment	Cooling method
1. Solution heat treatment	1320 °C/1 h+1325 °C/3 h+1335 °C/4 h	Air cooling
2. First-step aging heat treatment	1100 °C/6 h	Air cooling
3. Second-step aging heat treatment	870 °C/24 h	Air cooling
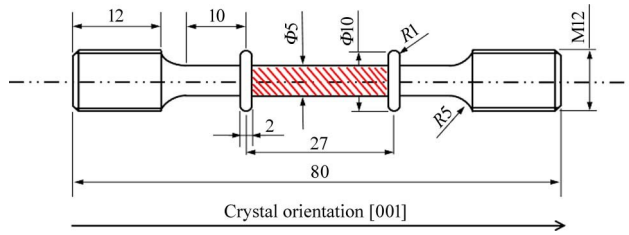
Fig.1 Schematic diagram of sample and location of Pt-Al coating

The metallographic samples were ground, polished, and finally etched at room temperature for $3-5$ s in the solution containing 4 g $CuSO_4$+10 mL HCl+20 mL H_2O. The phase composition of the outer coating samples was determined by X-ray diffractometer (XRD, D/max 2500Pc) using Cu Kα radiation source. Scanning electron microscope (SEM, Zeiss Merlin) was used to observe the fracture morphologies and cross-section microstructures. SEM equipped with electron backscattered diffractometer (EBSD) can also measure the grain size and average misorientation angle of the Pt-Al coatings through Channel 5 software. The chemical polishing solution (SiO_2) was used to grind and polish the coated or uncoated samples for 2 h before EBSD observation. EBSD patterns were obtained with scanning step size of 0.1 μm and accelerating voltage of 20 kV. Moreover, the high-angle grain boundaries were defined as the grain boundaries with neighboring grains misoriented by more than 10°. In order to minimize the effect of orientation in this research, the samples with misorientation angles within 10° were selected for analysis[28]. In addition to reducing the impact of orientation noise, which is related to the angular resolution of EBSD

equipment, boundaries were determined using a threshold angle of 2°. Transmission electron microscope (TEM, JEM 2100) was used to examine the cross-sectional substructure after the creep tests. The particular processes of TEM foil preparation inside the superalloy close to coating are shown in Ref.[29].

2 Results

2.1 Initial microstructure

SEM cross section morphology of the as-deposited Pt-Al coating before the creep test is shown in Fig.2a. The average thickness of the as-deposited Pt-Al coating is approximately 50 μm, and the Pt-Al coating exhibits a conventional bilayer structure. The outer layer of the Pt-Al coating is mainly composed of single-phase β-(Ni, Pt)Al layer, whereas the extensively precipitated interdiffusion zone (IDZ) is located in the inner layer. According to Fig. 2b, significantly coarser grains are present in the precipitate-lean β-(Ni, Pt)Al layer, compared with those in IDZ. After the coating thickness measurement through EBSD, the grain size variation of the β phase can be identified. Finer grains of the β phase exist in IDZ, because the precipitates impede the grain growth throughout the aluminizing diffusion process. XRD pattern of the outer coating layer is shown in Fig.2c. It can be found that the β-NiAl phase exists in Pt-Al coating, and it is abundant in nickel, platinum, and aluminum elements. The addition of platinum into β-NiAl can increase the lattice distortion and solidification of platinum, therefore forming the β-(Ni, Pt)Al single phase, which results in the modest leftward shift of the diffraction peaks, compared with the typical diffraction peaks of β-AlNi (PDF-44-1188) phase. Based on the ternary phase diagram of Al, Pt, and Ni[30], the existence of β-(Ni, Pt)Al
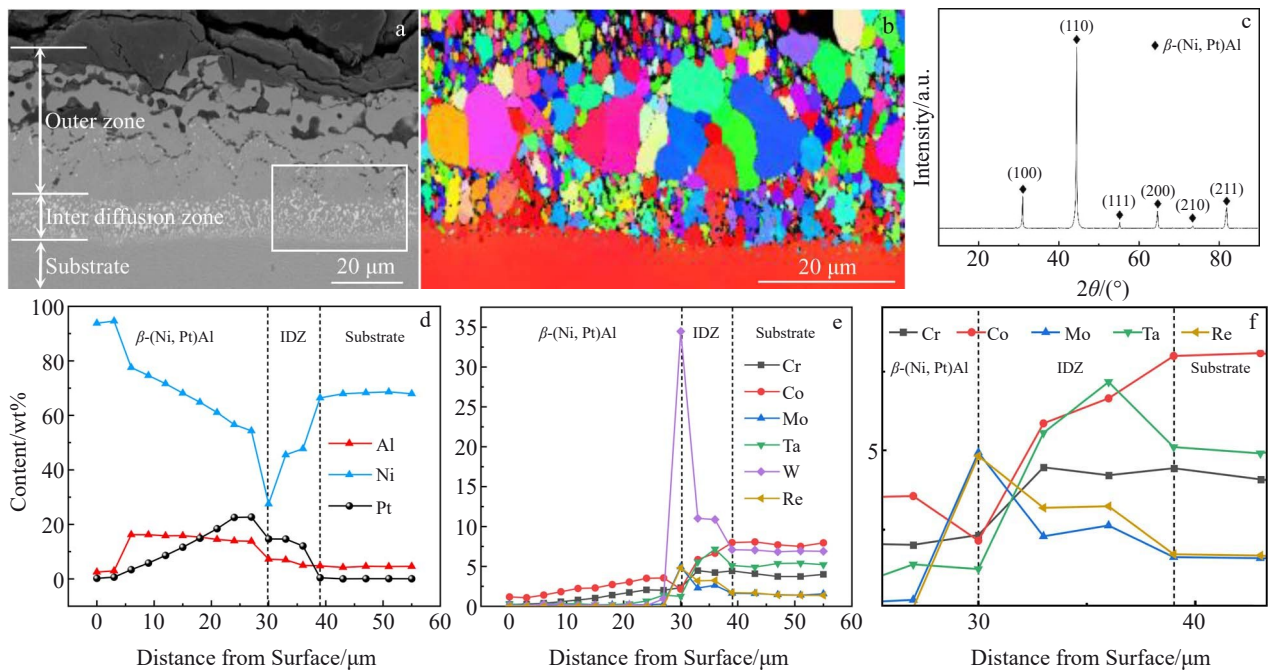
Fig.2 SEM cross section morphology of as-deposited Pt-Al coating (a); EBSD pattern of marked rectangular area in Fig.2a (b); XRD pattern of outer layer of Pt-Al coating (c); EDS analysis results of element contents across Pt-Al coating (d–f)

phase indicates that the components of Pt, Ni, and Al are situated in the β region. Tao et al[31] investigated the coating formation process from the surface of the original superalloy during the aluminizing diffusion process. Additionally, when the plating temperatures are higher than 1000 °C, the prepared Pt-Al coating grows outward, which promotes the formation of two-layer microstructure. During the preparation of β-(Ni, Pt)Al coatings, Ni element in the superalloy diffuses outward, forming a Ni-depleted zone, which is beneficial to IDZ. Ni consumption from the superalloy base during the aluminizing diffusion process alters the chemical potentials, so the chemical potential gradient appears for other elements. This phenomenon raises the element diffusivity. As a result, several precipitates are formed in IDZ, and the high-temperature strengthening elements (Co, Cr, W, Mo, Ta, and Re) are precipitated in multiple complex phases, as shown in Fig.2e.

As shown in Fig. 3a, no topologically close packed (TCP) phase occurs in the substrate close to the Pt-Al coating, whereas precipitation of the rafting phase does not occur. This can be attributed to the unique coating process, which hinders the diffusion of elements from the substrate to the coatings. Furthermore, it is found that the Pt-Al coated superalloy possesses the similar γ/γ' structure as the uncoated superalloy, as shown in Fig.3b.

2.2 Creep behavior

Creep curves of uncoated and Pt-Al coated SX superalloys under different creep conditions are shown in Fig. 4a and 4b, respectively. The creep curves of all samples show three stages with the secondary-tertiary creep stage as the main stage of the total creep process. The creep life results of uncoated and coated superalloy substrates under various creep conditions are illustrated in Fig. 4c. The creep life is also denoted as the time-to-rupture (TTR) term. Similar to the effect of Pt-Al coating on other second-generation SX
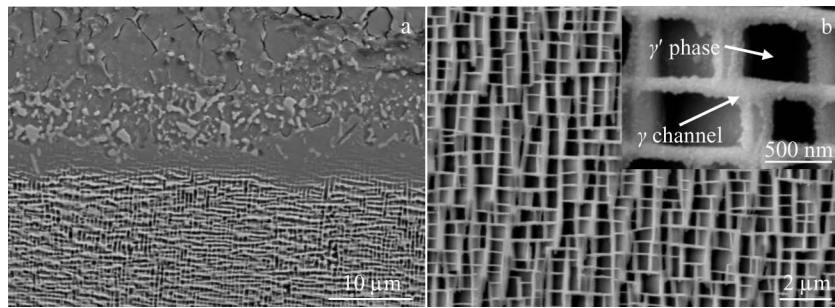

Fig.3   SEM microstructures of substrate close to (a) and far away from (b) Pt-Al coating
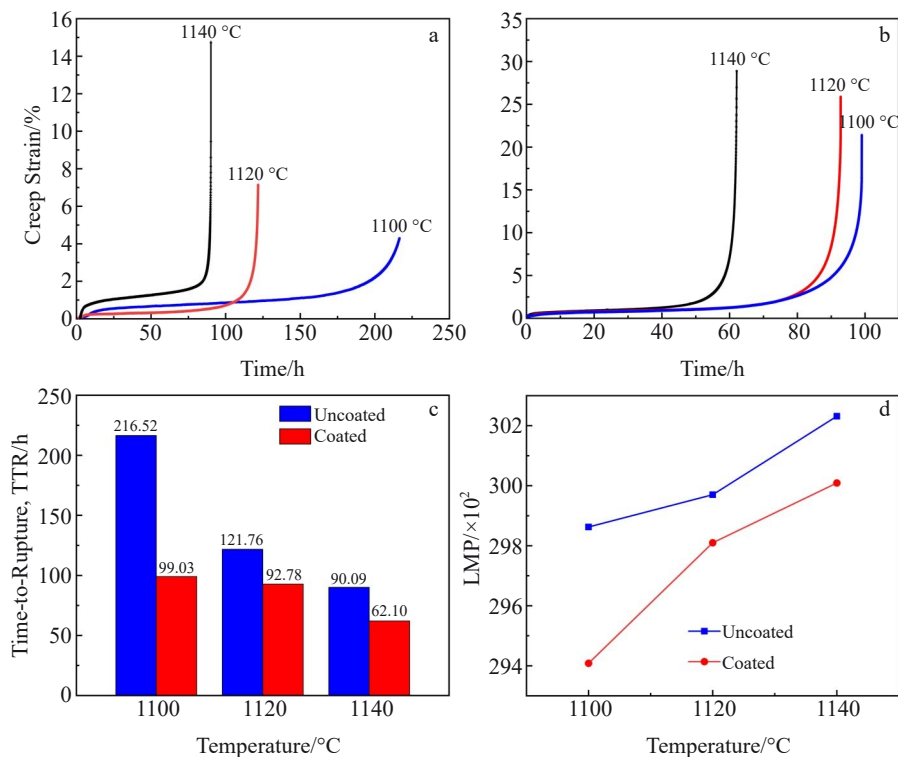

Fig.4   Creep life results of uncoated (a) and coated (b) superalloys; comparisons of TTR (c) and LMP (d) values between uncoated and coated superalloys

superalloys, the creep properties of Pt-Al coated superalloys are inferior to those of uncoated superalloys under all test conditions[32]. With the increase in applied temperatures from 1100 °C to 1140 °C, the decrement in creep life by coating can be reduced. When the applied temperature is 1100 °C, the creep life of the coated superalloy decreases by 50%, compared with that of uncoated superalloy, which is the most remarkable reduction in creep life among the applied conditions. Fig. 4d shows the Larsen-Miller parameter (LMP) of uncoated and coated superalloys to reflect their stress rupture response. LMP can be calculated through Eq. (1), as follows:

$$\text{LMP} = T\left(\lg t_f + C\right) \qquad (1)$$

where T is the applied temperature, t_f is TTR value, and C is a constant[33]. For superalloys, C is 20. According to Fig. 4d, the Pt-Al coated superalloys have lower LMP values than the uncoated superalloys do. It is evident that the creep behavior of superalloys deteriorates after coating with Pt-Al. The most obvious deterioration of LMP occurs when the test condition is 1100 °C/137 MPa.

In order to clearly show the changes of creep rate and time

in each stage during the creep process, the strain rate-creep life relationships are presented in Fig. 5. After analysis, the creep properties can be obtained, as listed in Table 3. The minimum creep rate of the coated samples is significantly lower than that of the uncoated superalloy under the same condition. Particularly, it decreases from 8.12×10^{-6} h^{-1} to 1.66×10^{-6} h^{-1} when the applied temperature is 1100 °C (T1 condition). However, the creep rate does not show significant changes between the uncoated and coated superalloys at 1120 and 1140 °C.

2.3 Fracture

The surface fracture characteristics of superalloys coated under different conditions are displayed in Fig. 6. As shown in Fig. 6a, 6d, and 6g, the superalloy substrate has a stepped quadrilateral structure, which suggests that the crack is initiated at the γ/γ' interface as a result of the alternate activation of the primary and secondary slip systems. A quasi-cracking surface in a rectangle shape is produced parallel to <110> by the crack propagation at the γ/γ' interface perpendicular to the primary uniaxial direction during creep tests. The uncoated samples also exhibit the similar features of stepped fracture[32].
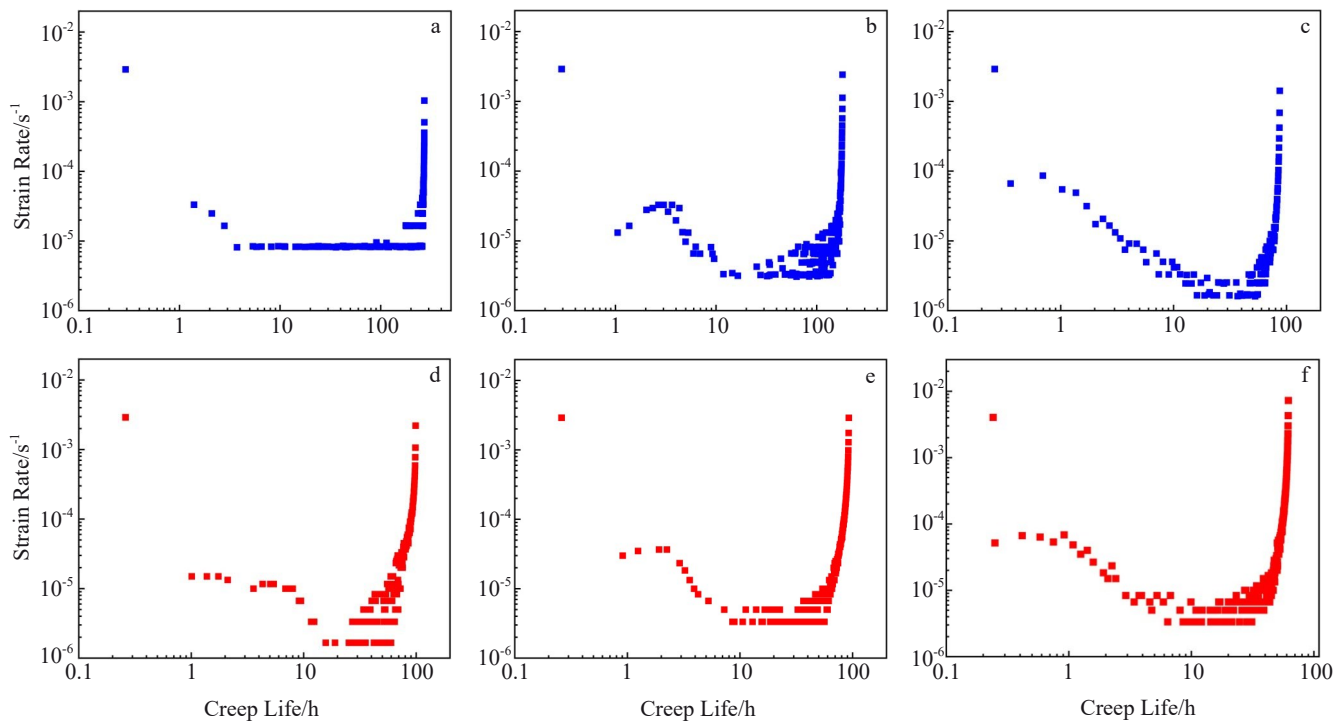

Fig.5　Strain rate-creep life relationships of uncoated (a–c) and coated (d–f) superalloys at 1100 °C (a, d), 1120 °C (b, e), and 1140 °C (c, f)

Table 3　Creep properties of uncoated and coated superalloys

| State	Condition	Creep life/h	Primary creep life/h	Secondary creep life/h	Tertiary creep life/h	Minimum creep rate/×10^{-6} h^{-1}
	T1	216.52	3.73±0.4	174.11±0.8	38.68±0.5	8.12±0.3
Uncoated	T2	121.76	3.33±0.2	75.85±0.6	42.58±0.5	3.34±0.2
	T3	90.09	7.38±0.4	66.33±0.5	16.38±0.6	2.53±0.3
	T1	99.03	15.67±0.5	58.31±0.7	25.05±0.4	1.66±0.2
Coated	T2	92.78	8.57±0.3	60.33±0.6	23.88±0.4	3.33±0.2
	T3	62.10	6.41±0.4	37.17±0.4	18.52±0.5	3.33±0.3
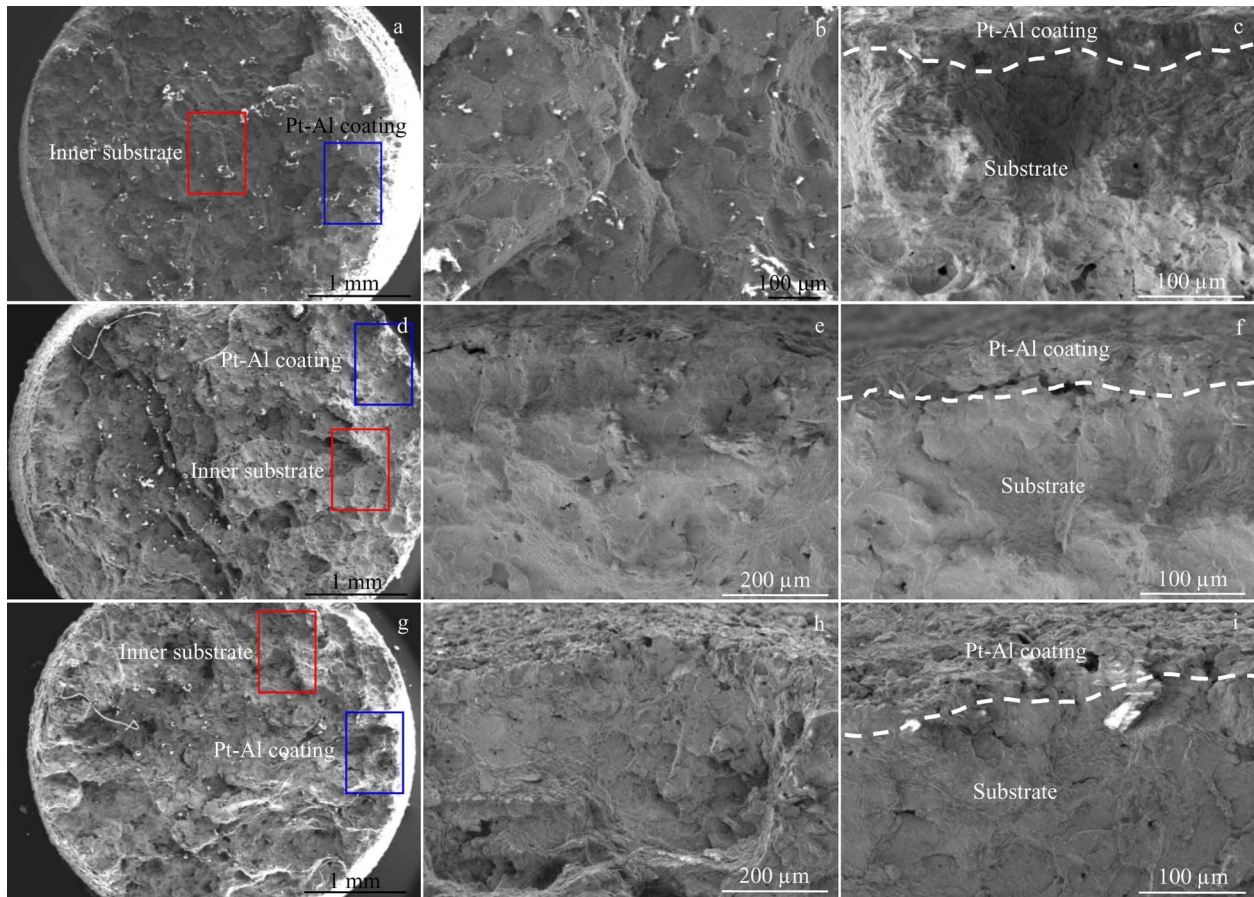
Fig.6 Morphologies of overall fracture surface (a, d, g), inner substrate in red rectangular areas (b, e, h), and Pt-Al coating in blue rectangular areas (c, f, i) of superalloys coated under T1 (a–c), T2 (d–f), and T3 (g–i) conditions after creep process

As shown in Fig. 6b, 6e, and 6h, the fracture surface of the superalloys exhibit shallow dimples. An oxidized layer is also formed around the fracture surface by exposure to high-temperature environment after failure.

Considering the Pt-Al coating, the fracture mechanism is micro-void coalescence in all three samples due to the existence of several micro-voids developed at the failure sites, as shown in Fig. 6c, 6f, and 6i. Based on the normal precipitates in the microstructure, voids exist in the coatings in every sample. However, at higher applied temperatures (Fig.6f and 6i), several elements from the coating promote the formation of a thin oxide layer on the fracture surface during exposure to high-temperature environment, which is not noticeable.

Longitudinal sections of failed superalloys coated under various conditions are presented in Fig.7a–7c. It can be found that the depth and width of the coating cracks under T1 condition are significantly larger than those under T2 and T3 conditions. According to Table 4, the depth and width of the coating cracks under T1 condition are twice as large as those under T2 condition and three times as large as those under T3 condition. Compared with that of the sample under T1 condition, the coating crack tip of the samples under T2 and T3 conditions undergoes different degrees of oxidation. The increase in applied temperature causes the coating to oxidize

at the crack tip, which slows down the propagation of cracks. Fig. 7d – 7i depict the coating crack section and its element composition analysis, revealing that oxidation causes cracks to propagate through the β -layer to IDZ. Therefore, the oxidation of coating cracks is closely related to the applied temperature and the composition of IDZ.

2.4 Deformation microstructure

The deformation microstructures of the superalloys near the Pt-Al coating were studied using bright-field TEM, as shown in Fig.8. Following results can be drawn. (1) The dislocation network of SX superalloy beneath the coating under T1 condition is looser than that under T2 and T3 conditions. The number of superdislocations cutting into the γ' phase under T1 condition is also larger than that under T2 and T3 conditions, as shown in Fig.8a. (2) Unlike the sample under T1 condition, fine secondary γ' phases can be observed in the samples under T2 and T3 conditions. This phenomenon can effectively impede the dislocation movement in the γ' phase, as presented in Fig.8b–8c. (3) Large-sized TCP phases can be observed in SX superalloy underneath the Pt-Al coating under T1 condition, as shown in Fig.8d–8f. These TCP phases promote the formation of dislocations, leading to the decrease in the strength, as illustrated in Fig. 8d. Therefore, the effect of applied temperature on the dislocations in superalloy substrate
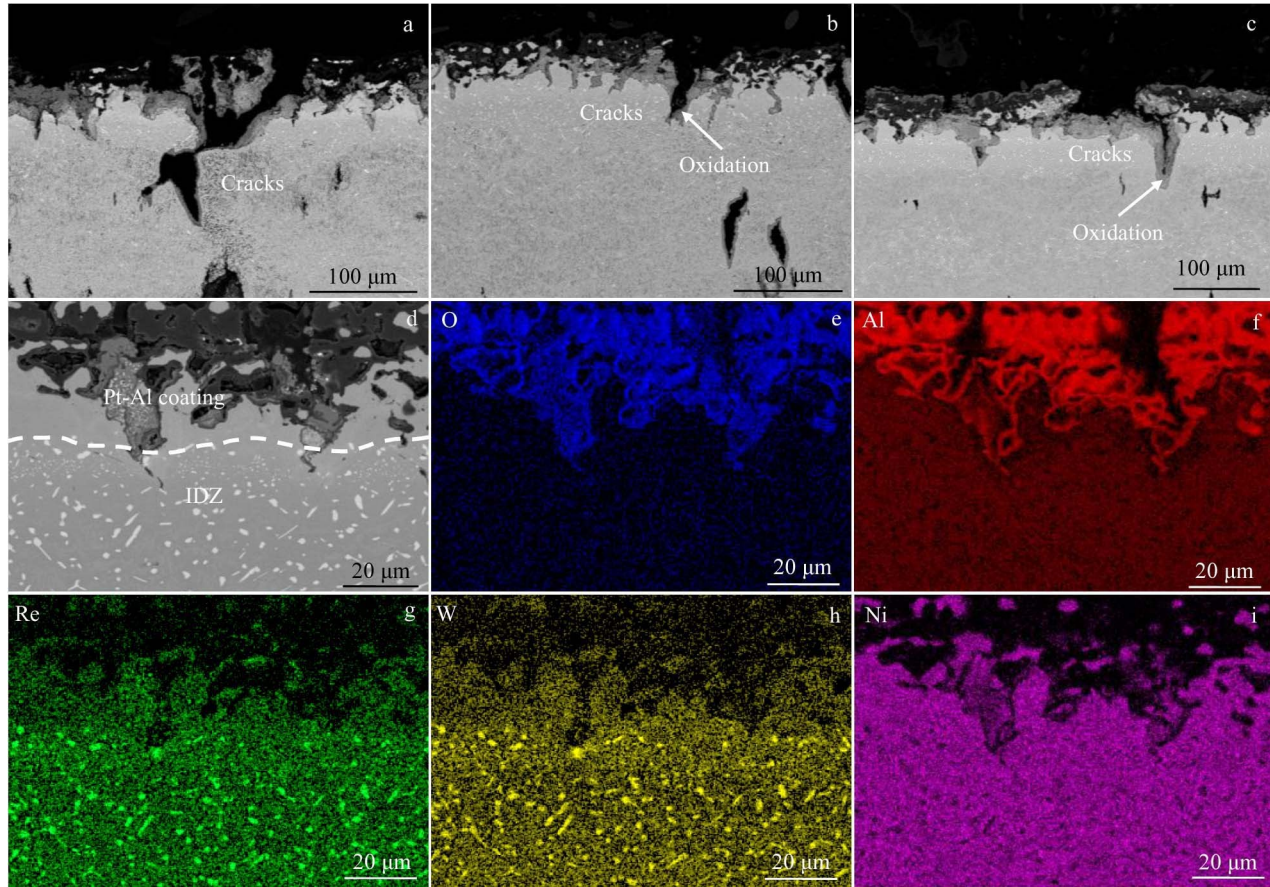
Fig.7   Longitudinal sections of failed superalloys coated under T1 (a), T2 (b), and T3 (c) conditions; SEM image (d) and corresponding EDS element mapping results (e–i) of Pt-Al coating under T2 condition: (e) O, (f) Al, (g) Re, (h) W, and (i) Ni

Table 4   Parameters of coating cracks near fracture surface under different creep conditions

Condition	Number of cracks	Width of coating cracks/μm	Depth of coating cracks/μm
T1	15±3	20±4	150±6
T2	6±3	10±3	70±6
T3	4±2	5±4	50±5

beneath the coatings under T2 and T3 conditions is less obvious than that under T1 condition.

3   Discussion

3.1   Crack oxidation mechanism

The creep performance of SX superalloys at elevated temperatures is significantly influenced by the oxidation protection zone (OPZ), which exists in Pt-Al coatings. Under T2 and T3 conditions, the coated surface is prone to cracking due to the formation of surface oxides at high temperatures. The rapid absorption of oxygen occurs through the air, interacting with the components to form oxides, such as NiO, CoO, Cr_2O_3, and Al_2O_3, on IDZ surface. These oxides have negative Gibbs free energies at the applied temperatures in this research, confirming the feasibility of oxide production within IDZ[33]. Due to its superior thermodynamic stability,

Al_2O_3 forms preferentially at the Pt-Al coated surfaces before oxidation. The cracks are initiated at Al_2O_3 sites and propagated throughout the coating during the high-temperature creep process. At the tips of the cracks, the formation of Al_2O_3 can also be observed. Besides, applying loading at high temperatures can increase the internal stress of oxides, and thus Al_2O_3 tends to spill. Furthermore, Ni and Co diffuse outward, forming new external oxide layer on IDZ of surface. In this case, a large amount of Co is enriched in IDZ, which causes its reaction with oxygen to produce trace amount of CoO. During the high-temperature exposure, the outer layers of IDZ are mainly composed of NiO and CoO oxides because they expand more rapidly, compared with other oxides[34]. Meanwhile, the oxygen reacts with Cr and Al, resulting in the formation of Cr_2O_3 and Al_2O_3, which penetrate the NiO and CoO layers. This process reduces the Ni outward diffusion and NiO growth. With the prolongation of exposure duration, Cr_2O_3 and Al_2O_3 are continuously synthesized, leading to the solid-state interactions between the inner Cr_2O_3 and Al_2O_3 and the outer NiO and CoO. This process results in the formation of spinel oxides, such as $NiCr_2O_4$, $NiAl_2O_4$, and $CoCr_2O_4$. All oxidized spinel reactions have negative Gibbs free energies, confirming the possibility of spinel structure formation. With the expansion of oxides, OPZ spreads across the SX substrate. The Ni and Co in the substrate diffuse
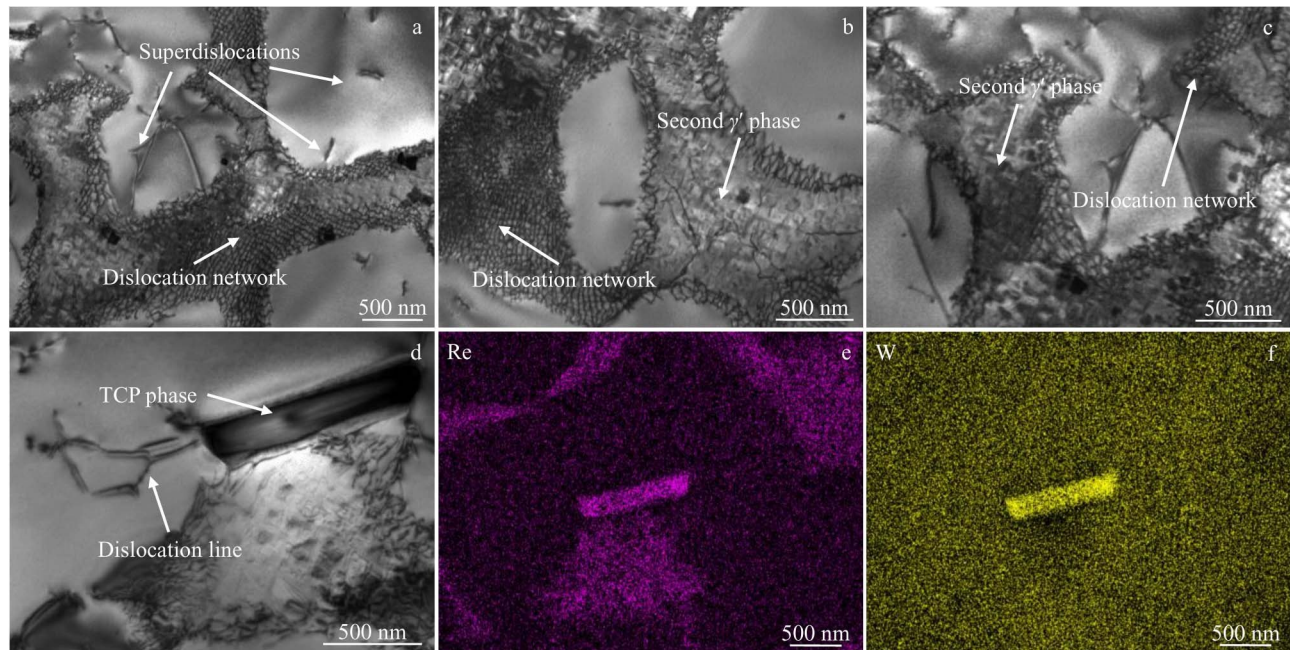
Fig.8　Bright-field TEM images of deformation microstructures of superalloys near Pt-Al coating prepared under T1 (a), T2 (b), and T3 (c) conditions; TEM image of TCP phase in superalloy under T1 condition (d); Re (e) and W (f) element mapping results of precipitates under T1 condition

outward towards the Cr_2O_3 and Al_2O_3 oxides, which is triggered by chemical potential gradient. Then, they come into contact with oxygen and form new NiO and CoO oxides. Ni diffuses more slowly and reacts with oxygen to produce NiO, forming the obvious multilayered oxide film structure. In contrast, Co preferentially diffuses towards OPZ of outer surface and interacts with the local oxides to form CoO due to its smaller dimensions and rapid diffusion velocity. A bumpy nickel oxide/spinel interface is produced when oxygen diffuses into the substrate and preferentially interacts with the nickel-rich region to from nickel-based oxides. The volume of NiO is increased with the oxidation process proceeding. Due to the lower strength (compared with that of adjacent CoO) and spinel oxides of NiO[35], extrusion occurs within the NiO, thereby forming micropores. Therefore, the formation of cracking oxides in the coatings prepared under T2 and T3 conditions is essential to inhibit further expansion of cracks towards coatings. Additionally, the mechanical properties of the substrate suffer less degradation in these cases. Fig. 9a shows the longitudinal section of the failed superalloy coated under T2 condition, which verifies the abovementioned mechanisms of oxidative passivation. At the same time, this oxidative passivation mechanism is also consistent with the results in Table 4.

3.2 Impact of applied temperatures on deformation mechanisms

With the increase in applied temperature, γ/γ' interfacial dislocation networks in the vicinity of the core superalloy are uniformly spaced, as shown in Fig. 8a – 8c. The γ substrate restricts the mobility of dislocation $a/2<110>$, which releases the misfit stress by ascending and gliding throughout the γ'

phase. High-density dislocation networks have ortho-hexagonal or tetragonal morphology, demonstrating the decline in dislocation splitting into the γ' precipitates. The well-distributed high-density interfacial dislocation networks may drastically restrict the creep rate, producing apparent γ/γ' interfacial strengthening effect. However, the structure of the dislocation network is irregular and wave-shaped in the substrate region adjacent to the coating. The development of an erratic dislocation network is mainly caused by element diffusion-induced low lattice misfit[36]. At the binding layer/substrate interface, the solidifying elements (Co, Mo, W, and Re) in the γ' precipitation phase diffuse outward into the binding layer, and both γ' and TCP phases are greatly precipitated during the high-temperature creep process. Depletion of γ/γ' results in a reduction of the lattice misfit by decreasing the lattice constant gap between γ matrix and γ' precipitation, based on the relationship $|\delta|=2(a\gamma'-a\gamma)/(a\gamma'+a\gamma)$. The creep properties of the coated samples are improved as a result of the weakened pinning effect caused by the uneven dislocation network with low mismatch[37]. It is fascinating to note that the precipitated γ' phase under T1 condition contains an enormous quantity of dislocation debris. This is caused by the elements diffusing from the γ' precipitates due to component segregation via TCP phase precipitation at the interface and element depletion by the coating, which decreases the solution strengthening of the γ' precipitates near the coating. Within the γ' phases, debris can appear due to the dislocations slipping into the weakened γ' structures. However, under T2 and T3 conditions, the large consumption of Al within the coating by surface and crack oxidation reduces the chemical potential gradient between the coating
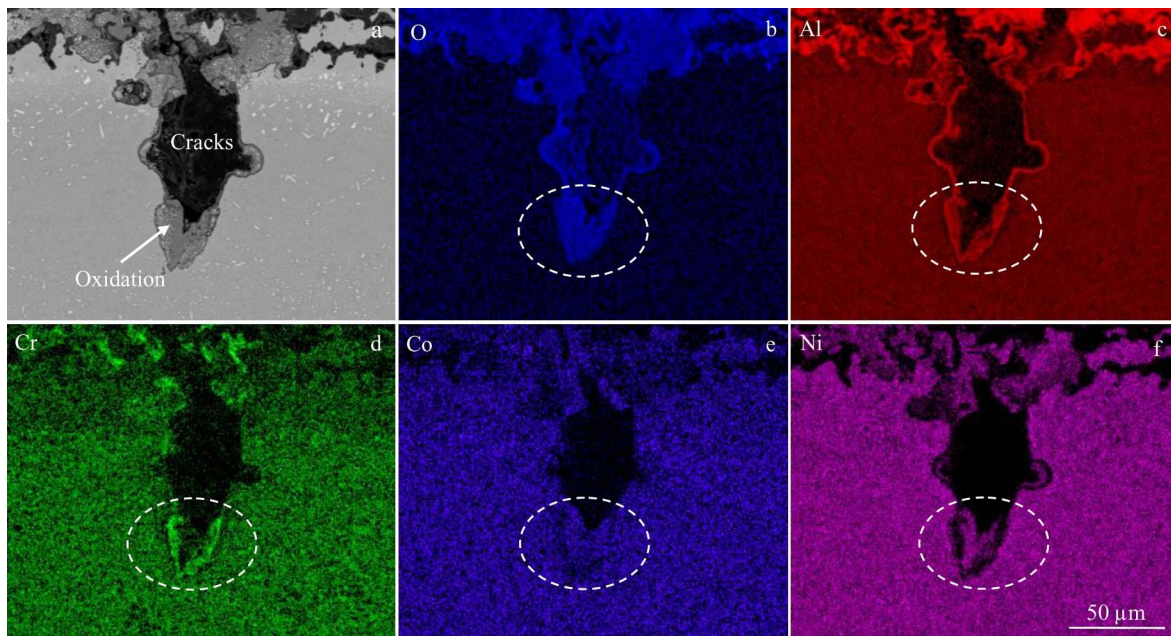
Fig.9 SEM longitudinal section (a) and corresponding EDS element distributions (b−f) of failed superalloy coated under T2 condition: (b) O, (c) Al, (d) Cr, (e) Co, and (f) Ni

and the substrate, slowing down the diffusion of Al atoms, therefore enhancing the microstructure stability, and inhibiting the formation of TCP phase in the substrates beneath the coatings.

The morphologies of the secondary γ' phases and their development in the superalloys coated under T2 and T3 conditions are shown in Fig. 8b and 8c, respectively. Under these conditions, there is sufficient time for atomic diffusion to reach the chemical equilibrium, so the diffusion and partitioning of residual formation elements, such as Al and Ta, in the γ substrate promote the nucleation of a certain number of fine secondary γ' phases[38]. The abovementioned mechanism is regulated by uphill diffusion, because the substrate does not contain any γ'-rich components. Nucleation is more likely to occur in the regions far from the γ/γ' interface, where Al and Ta atoms are mostly depleted. Once the nucleation process ceases, the Al and Ta atoms diffuse and form the secondary γ' phase. But under this circumstance, the secondary γ' phases of the superalloy under the Pt-Al coating cannot form precipitates in the γ channels. Owing to the substantially faster migration rates of the secondary γ' precipitates, the γ-rich components are mainly released from the precipitates through the dislocation pipe channels[39]. However, the infusion of these elements from the γ substrate and their enhanced pipe transit are crucial for the migration of the γ-rich elements (Al and Ta) towards the precipitates[40]. Because of their outward diffusion, the total number of Ta and Co-rich components in the γ channel decreases, which delays the nucleation of the secondary γ' phase and hampers the development of the secondary γ' phase. As a result, it is improbable that the secondary γ' phase can appear at the superalloy substrate beneath the Pt-Al coating. Generally, the

formation of the secondary γ' phase at high temperatures can partially obstruct the dislocation motion in the γ matrix[41]. Hence, the Pt-Al coating leads to the depletion of the secondary γ' phase in the superalloy substrate, which reduces the resistance against dislocation motion and further reduces the creep strength of the coating under T1 condition.

3.3 Impact of applied temperatures on mechanical degradation

Based on the abovementioned discussion, it can be concluded that the mechanical property damage on the coatings prepared under T2 and T3 conditions on SX superalloy substrate is slighter than that under T1 condition. The main reasons are as follows. (1) With the increase in applied temperature, the β phase coating becomes tougher and has better co-deformation ability with the SX superalloy substrate, which decreases the possibility of crack initiation. (2) The rise in applied temperature triggers the oxidation of the crack tip of coatings prepared under T2 and T3 conditions. This oxidation can effectively hinder the further spread of cracks within the coating. Besides, the lower applied temperature in T1 condition results in the weaker oxidation effect on cracks. (3) The coatings prepared under T2 and T3 conditions tend to consume all Al atoms, leading to the decline in the mechanical properties of both the coating and the SX superalloy substrate. When the coatings prepared under T2 and T3 conditions suffer crack oxidation, they deplete Al atoms within the coatings, which in turn reduces the chemical potential gradient between the coating and the SX superalloy substrate. Thus, even though the applied temperatures of T2 and T3 conditions are higher than that of T1 condition, the microstructure stability of coatings prepared under T2 and T3 conditions is greater than that under T1

condition. The degradation of β phases is reflected by the existence of a large number of γ' phases within the coating prepared under T1 condition, and the γ' phase in the substrate degrades into the β phase, which also leads to the appearance of deleterious TCP phases at the interface between the coating and SX superalloy substrate. (4) The severe element diffusion in the coating prepared under T1 condition also leads to the decrease in the dislocation mesh density and the increase in the number of superdislocations cutting into the γ' phase of the SX superalloy substrate, which significantly reduces the bonding strength between the coating and SX superalloy substrate. (5) The higher applied temperatures also result in the formation of the secondary γ' phases at the coating/SX superalloy substrate interface, which can impede the movement of substrate dislocations and enhance the high-temperature strength of SX substrate beneath the coatings prepared under T2 and T3 conditions. These reasons jointly result in the more severe mechanical damage of T1 treatment condition to the SX superalloy substrate, compared with those of T2 and T3 conditions.

4 Conclusions

1) The Pt-Al coating has two layers and consists of IDZ of refractory metal precipitates. The outer layer is composed of β-(Ni, Pt)Al single brittle phase. The superalloy area adjacent to coating does not has any rafting γ' or TCP phase, suggesting that the coating and substrate are well-matched.

2) The superalloys coated under all three conditions have slightly worse creep performance, compared with those of uncoated superalloys. With the increase in applied temperature, the reduction in creep life by coating is minimized. The most significant decrease in creep life occurs under T1 condition (1100 °C/137 MPa). The creep life of coated superalloys is shorter than that of uncoated superalloys by approximately 50%.

3) The increase in applied temperatures to 1120 and 1140 °C causes the oxidation of the coating crack tip. This phenomenon can effectively hinder the internal propagation of the coating cracks.

4) When the applied temperature increases to 1120 °C, the density of the dislocation network decreases, and the total number of superdislocations cutting into the γ' phase of SX superalloy substrate beneath the coating increases. The higher temperatures also cause the formation of the secondary γ' phases at the coating/SX superalloy substrate interface, which can hinder the movement of dislocations.

References

1   Tan Z H, Wang X G, Song W *et al*. *Vacuum*[J], 2020, 175: 109284

2   Li W Q, Zhao X B, Xu J C *et al*. *Vacuum*[J], 2023, 209: 111780

3   Lai Yongjun, Ning Likui, Zhao Ling *et al*. *Rare Metal Materials and Engineering*[J], 2024, 53(3): 748 (in Chinese)

4   Li Yanqiong, Zhang Junmin, Guan Werming *et al*. *Rare Metal Materials and Engineering*[J], 2010, 39(10): 1727 (in Chinese)

5   Long H B, Mao S C, Liu Y N *et al*. *Acta Materialia*[J], 2020, 185: 233

6   Li D Q, Guo H B, Guo D *et al*. *Corrosion Science*[J], 2013, 66: 125

7   Svensson H, Christensen M, Knutsson P *et al*. *Corrosion Science*[J], 2009, 51(3): 539

8   Esakkiraja N, Gupta A, Jayaram V *et al*. *Acta Materialia*[J], 2020, 195: 35

9   Liu R D, Jiang S M, Jiang C Q *et al*. *Corrosion Science*[J], 2017, 120: 121

10 Bai B, Guo H B, Peng H *et al*. *Corrosion Science*[J], 2011, 53(9): 2721

11 Tian T, Hao Z B, Ge C C *et al*. *Materials Science and Engineering A*[J], 2020, 776: 139007

12 Sohrabi M J, Mirzadeh H. *Vacuum*[J], 2019, 169: 108875

13 Das D K. *Progress in Materials Science*[J], 2013, 58(2):151

14 Latief F H, Kakehi K. *Materials & Design*[J], 2014, 56: 816

15 Jiang C Y, Li S, Liu H *et al*. *Corrosion Science*[J], 2019, 166: 108424

16 Yang Y F, Jiang C Y, Yao H R *et al*. *Corrosion Science*[J], 2016, 113: 17

17 Han B H, Ma Y, Peng H *et al*. *Corrosion Science*[J], 2016, 102: 222

18 Li W, Sun J, Liu S B *et al*. *Corrosion Science*[J], 2020, 164: 108354

19 Li W, Fu L B, Liu Y D *et al*. *Corrosion Science*[J], 2020, 176: 108892

20 GB/T 2039-2012, ISO 204[S], 2009

21 Lei Y B, Wang Z B, Xu J L *et al*. *Acta Materialia*[J], 2019, 15: 133

22 Hayashi S, Ford S I, Young D J *et al*. *Acta Materialia*[J], 2005, 53: 19

23 Pichoir R. *ONERA*[J], 1978, 143: 271

24 Zhang Z K, Zhang Z F. *Journal of Alloys and Compounds*[J], 2018, 746: 84

25 Ma S, Carroll L, Pollock T M. *Acta Materialia*[J], 2007, 55(17): 5802

26 Tao X P, Wang X G, Meng J *et al*. *Engineering Failure Analysis*[J], 2022, 133: 105963

27 Yang Y F, Jiang C Y, Bao Z B *et al*. *Corrosion Science*[J], 2016, 106: 43

28 Du Y L, Tan Z H, Yang Y H *et al*. *Rare Metal Materials and Engineering*[J], 2021, 50(4): 1132

29 Tao X P, Wang X G, Zhou Y Z *et al*. *Journal of Materials Research and Technology*[J], 2021, 14: 567

30 Gleeson B, Wang W, Hayashi S *et al*. *Materials Science Forum*[J], 2004, 461: 213

31 Tao X P, Tao X G, Zhou Y Z *et al*. *Materials Science and Engineering A*[J], 2021, 805: 140575

32 Yu Z Y, Wang X Z, Yue Z F *et al*. *Materials Science and*

Engineering A[J], 2017, 697: 126

33 Tao X P, Wang X G, Zhou Y Z. *Surface and Coating Technology*[J], 2020, 389: 125640

34 Gui Y T, Zhao M, Jiang P *et al. Corrosion Science*[J], 2023, 223: 111464

35 Li T, Li Y, Li W *et al. Vacuum*[J], 2023, 212: 112025

36 Taylor M P, Evans H E, Busso E P *et al. Acta Materialia*[J], 2006, 54: 3421

37 Yang W C, Qu P F, Sun J C *et al. Vacuum*[J], 2020, 181: 109682

38 He C, Liu L, Huang T *et al. Journal of Alloys and Compounds*[J], 2020, 836: 155486

39 Tao X P, Tan K J, Liang J J *et al. Materials & Design*[J], 2023, 229: 111880

40 Li Y F, Wang L, Zhang G *et al. Materials Science and Engineering A*[J], 2019, 760: 26

41 Tao X P, Du Y L, Wang X G *et al. Journal of Materials Science and Technology*[J], 2022, 131: 14

温度对**Pt-Al**涂层第三代低成本单晶高温合金蠕变行为的影响

张　舸 [1]，陶稀鹏 [2]，Syed Muhammad Abbas Jafri [2]，王新广 [2]，张　松 [1]，张春华 [1]，
梁静静 [2]，李金国 [2]，孙晓峰 [2]，周亦胄 [2]

(1. 沈阳工业大学 材料科学与工程学院，辽宁 沈阳 110870)
(2. 中国科学院 金属研究所 师昌绪先进材料创新中心，辽宁 沈阳 110016)

摘　要：探究了应用温度对含 Pt-Al 涂层的第三代低成本单晶高温合金蠕变行为的影响。在 1100 ℃/137 MPa、1120 ℃/137 MPa 和 1140 ℃/137 MPa条件下观察蠕变损伤。结果表明：在所有测试条件中，裸基体高温合金均优于带涂层高温合金。在 1100 ℃/137 MPa 下进行测试时，蠕变寿命最明显地缩短了50%。在更高温度（1120 和 1140 ℃）下，Pt-Al 涂层向单晶高温合金基体的裂纹扩展速度减慢，从而减少了力学性能的下降，涂层裂纹的尖端氧化和铝扩散形成了氧化物，而不是渗透到单晶基体中，导致涂层下基体的微结构退化缓慢。然而在 1100 ℃时，涂层/单晶合金基底的微观结构由于铝的内部扩散而退化。这种扩散机制使有害的拓扑密堆相在 1100 ℃左右形成。在 1120 和 1140 ℃时，涂层下单晶合金基底的位错与内部高温合金的位错相比保持相对不变。与此相反，涂层下基底的位错网络变得稀疏，在 1100 ℃时切割成相的超位错数量增加。

关键词：Pt-Al涂层；高温蠕变；单晶高温合金；裂纹氧化；微观结构演变

作者简介：张　舸，男，1998年生，硕士生，沈阳工业大学材料科学与工程学院，辽宁 沈阳 110870，E-mail：15942069690@163.com